Inorganic Chemistry
Article

Inorg. Chem. **2010**, *49*, 9839–9851 **9839**
DOI: 10.1021/ic100364v

Case Study on a Rare Effect: The Experimental and Theoretical Analysis of a Manganese(III) Spin-Crossover System

Shi Wang,*,† Marilena Ferbinteanu,*,‡ Crina Marinescu,‡ Alexandra Dobrinescu,§ Qi-Dan Ling,† and Wei Huang*,†

†*Jiangsu Key Laboratory of Organic Electronics & Information Displays and Institute of Advanced Materials (IAM), Nanjing University of Posts and Telecommunications, Nanjing 210046, People's Republic of China,* ‡*Inorganic Chemistry Department, Faculty of Chemistry, University of Bucharest, Dumbrava Rosie 23, Bucharest 020462, Romania, and* §*Department of Physics, "A. I. Cuza" University, Iasi 700506, Romania*

Received February 23, 2010

The six-coordinated mononuclear manganese(III) complex [Mn(5-Br-sal-N-1,5,8,12)]ClO_4 has been synthesized and isolated in crystalline form. Magnetic measurements and variable-temperature single-crystal X-ray crystallography corroborated with theoretical analysis provided firm evidence for the spin-crossover effects of this system. The monomeric complex cations are made by a hexadentate mixed-donor Schiff base ligand imposing a distorted octahedral geometry and subtle structural effects determining the manifestation of the variable spin properties of the manganese(III) centers. The spin crossover in [Mn(5-Br-sal-N-1,5,8,12)]ClO_4 has resulted in an unprecedented crystallographic observation of the coexistence of high-spin (HS; $S = 2$) and low-spin (LS; $S = 1$) manganese(III) complex cations in equal proportions around 100 K. At room temperature, the two crystallographically distinct manganese centers are both HS. Only one of the two slightly different units undergoes spin crossover in the temperature range ~250−50 K, whereas the other remains in the HS state down to 50 K. The density functional theory calculations, performed as relevant numerical experiments designed to identify the role of orbital and interelectron effects, revealed unedited aspects of the manganese(III) spin-conversion mechanisms, developed in the conceptual frame of ligand-field models.

Introduction

Aside from being a rather fascinating phenomenon for academic insight, as a transformation having a driving force practically at the atomic level, inside the metal ions whose complexes are exhibiting it, the spin-crossover (SCO) phenomenon[1] brings significant appeal to potential applications in materials science. It is a firm example of bistability,[2,3] implying that tunable electronic structure transformations change, along with the molecular ground state, all of the displayed optical and magnetic properties. Consequently, SCO is a good candidate for new technologies of information processing and storage, with the two distinct states of the system playing the role of 0 and 1 bits in handling and recording data.

The most representative situation is the temperature-dependent SCO behavior,[4] which implies a transition from a low-spin (LS) state to a high-spin (HS) one, upon heating, reversible at cooling, in certain cases with good hysteresis separating the up and down sweep modes.[5,6] Numerous studies revealed a variety of other perturbations that can tune the transition: pressure,[7] irradiation,[8,9] or external magnetic field.[1,10]

Although, on the grounds of the basic concepts of ligand-field theory,[11] the SCO phenomenon is, in principle, possible for octahedral d^4−^{7} ions, the vast majority of the reported SCO complexes are iron coordination compounds [iron(II)

*To whom correspondence should be addressed. E-mail: iamswang@njupt.edu.cn (S.W.), marilena.cimpoesu@g.unibuc.ro (M.F.), wei-huang@njupt.edu.cn (W.H.).

(1) Gütlich, P.; Goodwin, H. A. Spin Crossover in Transition Metal Compounds I. *Topics in Current Chemistry*; Springer: Berlin, 2004; Vol. *233*, pp 1−47.
(2) Adams, D. A.; Dei, A.; Rheingold, A. L.; Hendrickson, D. N. *J. Am. Chem. Soc.* **1993**, *115*, 8221–8229.
(3) Kahn, O.; Martinez, C. J. *Science* **1998**, *279*, 44–48.
(4) Gütlich, P.; Hauser, A.; Spiering, H. *Angew. Chem., Int. Ed.* **1994**, *33*, 2024–2054.
(5) Tanasa, R.; Enachescu, C.; Stancu, A.; Linares, J.; Codjovi, E.; Varret, F.; Haasnoot, J. *J. Phys. Rev. B* **2005**, *71*, 014431.
(6) Weber, B.; Kaps, E. S.; Obel, J.; Achterhold, K.; Parak, F. G. *Inorg. Chem.* **2008**, *47*, 10779–10787.
(7) Gütlich, P.; Ksenofontov, V.; Gaspar, A. B. *Coord. Chem. Rev.* **2005**, *249*, 1811–1829.
(8) Hauser, A. *Top. Curr. Chem.* **2004**, *234*, 155–198.
(9) Shimamoto, N.; Ohkosi, S. I.; Sato, O.; Hashimoto, K. *Inorg. Chem.* **2002**, *41*, 678–684.
(10) Varret, F.; Bleuzen, A.; Boukheddaden, K.; Bousseksou, A.; Codjovi, E.; Enachescu, C.; Goujon, A.; Linares, J.; Menendez, N.; Verdaguer, M. *Pure Appl. Chem.* **2002**, *74*, 2159–2168.
(11) (a) Figgis, B. N. *Introduction to Ligand Field*; Interscience Publishers: New York, 1966. (b) Figgis, B. N.; Hitchman, M. A. *Ligand Field Theory and Its Applications*; Wiley-VCH: New York, 2000. (c) Lever, A. B. P. *Inorganic Electronic Spectroscopy*, 2nd ed.; Elsevier Publishing Co.: Amsterdam, The Netherlands, 1984. (d) Solomon, E. I.; Lever, A. B. P. *Inorganic Electronic Structure and Spectroscopy*; John Wiley & Sons: New York, 1999.

Published on Web 09/30/2010

Scheme 1

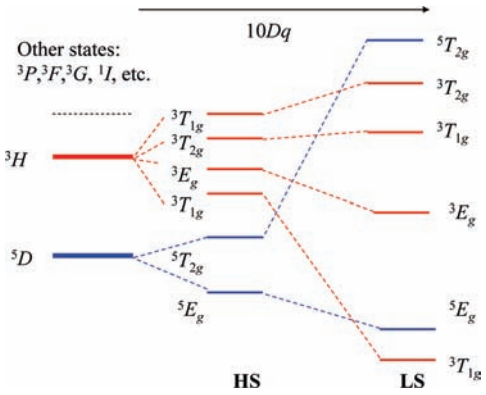

more frequently than iron(III)], to a lesser extent cobalt(II), and only in a few cases chromium(II) or manganese(III).[12] The spin transitions in d^4 ions are the rarest.[13] The particularities of the actual Schiff base ligand favor the occurrence of the SCO event in our manganese(III) system, providing a good opportunity to study the factors of this rare effect.

Because the actual LS state of manganese(III), $S = 1$, is, in fact, an intermediate spin (the lowest one being the unreachable $S = 0$ configuration), the actual conversion can also be called an intermediate-spin (IS) case. However, in order to avoid confusion due to the less popular IS acronym, we will use throughout the paper the usual HS and LS tags. A qualitative representation of the lowest spectral terms involved in the d^4 SCO is given in Scheme 1.

Beyond the basic interpretation of the spin transition as a balance between the ligand-field stabilization energy (LFSE) and electron-pairing costs, the spin conversion is also subtly and essentially determined by the interplay of intermolecular effects. The lattice vibrations interact with distortion modes of the coordination sphere, determining, at a critical point, the switch of the ground state.[14] The coupling between molecular and intermolecular movements determines the cooperativity effect, which is the prerequisite for the apparition of hysteresis. The hysteretic manifestations are desirable because they afford a good instrumental discrimination of the HS and LS states in the potentially new technologies based on this sort of bistability. The best candidates for sharp and hysteretic SCO effects can be found among the iron(II) complexes.[6] Most of the iron(III) SCO complexes, practically all of the cobalt(II) ones, and very few manganese(III) SCO species show only gradual spin conversion, without hysteresis. As matter of conventional terminology, the sharp SCO manifestations can be named spin transitions, while the gradual ones are better called spin conversions. The SCO term is commonly adequate for both transition and gradual conversion cases because it refers to the causal root that drives both types of manifestations. A challenging open question is, why are the iron(II) systems best suited for definite spin-transition hysteretic effects, while the other ions are limited to the gradual conversion occurrence?

For an idealized octahedral d^4 system, which can be described in terms of the ligand field ($10Dq$) and the Racah (B and C) interelectronic parameters,[15] the condition for crossing between the ^5E_g and $^3T_{1g}$ terms is, in a crude estimation, $10Dq \sim 6B + 5C$ (see the Supporting Information). Further simplification is done by introducing acknowledged approximate relationships,[16] such as $C \sim 4B$ or $C \sim 4.5B$, obtaining the $10Dq \sim 26B$ or $28.5B$ condition. A more complete description is realized by modeling the full configuration interaction (CI) and drawing the corresponding Tanabe−Sugano diagrams,[16] which, at closer examination, support the above approximation of the crossing point. Compared with the approximate crossover condition for d^6 ions, $10\ Dq \sim 2.5B + 4C$, it seems that the d^4 SCO demands higher fields. The quintet−singlet crossing demands higher fields, being practically unreachable. One may speculate that the relative unavailability of rather extreme strong ligand-field environments and the absence of accessible singlet states is the possible explanation for the scarcity of the SCO for manganese(III) systems.

The success of the present work in obtaining a d^4 spin-conversion effect seems to be due to the ligand-field strength of the actual ligand, cumulating six strong donors in one single organic skeleton. This type of Schiff base with a *trans*-N_4O_2 set of donors was first encountered in iron(III) SCO complexes, in solution, near room temperature,[17] which made them ideal subjects for the study of kinetics of HS → LS spin relaxation in solution,[18] and the influence of spin-state changes on the iron(III/II) redox couples.[19] More recently, their derivatives have been incorporated into metal−organic/inorganic hybrid material[20] and potentially switchable molecular conductors[21] and used as spectroscopic models for ferric biosites.[22] Notably, although some derivatives undergo SCO in solution, in the solid state their magnetic behavior is very variable, ranging from HS through SCO, incomplete SCO, to LS.[23] The Schiff base ligands are frequent encounters in the

(12) Murray, K. S. *Eur. J. Inorg. Chem.* **2008**, 3101–3121.
(13) (a) Garcia, Y.; Gütlich, P. In Spin Crossover in Transition Metal Compounds II. *Topics in Current Chemistry*; Gülich, P., Goodwin, H. A., Eds.; Springer-Verlag: Berlin, 2004; Vol. *234*, pp 49−62. (b) Liu, Z.; Liang, S.; Di, X.; Zhang, J. *Inorg. Chem. Commun.* **2008**, *11*, 783–786.
(14) (a) Spiering, H.; Boukheddaden, H.; Linares, J.; Varret, F. *Phys. Rev. B* **2004**, *70*, 184. (b) Spiering, H.; Meissner, E.; Köppen, H.; Müller, E. W.; Gütlich, P. *Chem. Phys.* **1982**, *68*, 65.
(15) Racah, G. *Phys. Rev.* **1942**, *62*, 438–462.
(16) Tanabe, Y.; Sugano, S. *J. Phys. Soc. Jpn.* **1954**, *9*, 766–779.
(17) Tweedle, M. F.; Wilson, L. J. *J. Am. Chem. Soc.* **1976**, *98*, 4824–4834.
(18) (a) Dose, E. V.; Hoselton, M. A.; Sutin, N.; Tweedle, M. F.; Wilson, L. J. *J. Am. Chem. Soc.* **1978**, *100*, 1141–1147. (b) Binstead, R. A.; Beattie, J. K.; Dose, E. V.; Tweedle, M. F.; Wilson, L. J. *J. Am. Chem. Soc.* **1978**, *100*, 5609–5614. (c) Binstead, R. A.; Beattie, J. K.; Dewey, T. G.; Turner, D. H. *J. Am. Chem. Soc.* **1980**, *102*, 6442–6451. (d) Lawthers, I.; McGarvey, J. J. *J. Am. Chem. Soc.* **1984**, *106*, 4280–4282. (e) Schenker, S.; Hauser, A.; Dyson, R. M. *Inorg. Chem.* **1996**, *35*, 4676–4682.
(19) (a) Kadish, K. M.; Das, K.; Schaeper, D.; Merrill, L.; Welch, B. R.; Wilson, L. J. *Inorg. Chem.* **1980**, *19*, 2816–2821. (b) Kadish, K. M.; Su, C. H.; Wilson, L. J. *Inorg. Chem.* **1982**, *21*, 2312–2314. (c) Zhu, T.; Su, C. H.; Schaeper, D.; Lemke, B. K.; Wilson, L. J.; Kadish, K. M. *Inorg. Chem.* **1984**, *23*, 4345–4349.
(20) (a) Floquet, S.; Muñoz, M. C.; Rivière, E.; Clément, R.; Audière, J.-P.; Boillot, M.-L. *New J. Chem.* **2004**, *28*, 535–541. (b) Nakano, M.; Nakahama, A.; Okuno, S.; Matsubayashi, G.-E.; Mori, W.; Katada, M. *Mol. Cryst. Liq. Cryst.* **2002**, *376*, 399–404. (c) Floquet, S.; Salunke, S.; Boillot, M.-L.; Clément, R.; Varret, F.; Boukheddaden, K.; Rivière, E. *Chem. Mater.* **2002**, *14*, 4164–4171. (d) Jaiswal, A.; Floquet, S.; Boillot, M.-L.; Delhaes, P. *Chem. Phys. Chem.* **2002**, *3*, 1045–1049.
(21) (a) Dorbes, S.; Valade, L.; Real, J. A.; Faulmann, C. *Chem. Commun.* **2005**, 69–71. (b) Faulmann, C.; Dorbes, S.; Real, J. A.; Valade, L. *J. Low Temp. Phys.* **2006**, *142*, 261–266. (c) Pereira, L. C. J.; Gulamhussen, A. M.; Dias, J. C.; Santos, I. C.; Almeida, M. *Inorg. Chim. Acta* **2007**, *360*, 3887–3895. (d) Takahashi, K.; Cui, H.-B.; Okano, Y.; Kobayashi, H.; Mori, H.; Tajima, H.; Einaga, Y.; Sato, O. *J. Am. Chem. Soc.* **2008**, *130*, 6688–6689.
(22) Carrano, C. J.; Carrano, M. W.; Sharma, K.; Backes, G.; Sanders-Loehr, J. *Inorg. Chem.* **1990**, *29*, 1865–1870.
(23) (a) Nishida, Y.; Kino, K.; Kida, S. *J. Chem. Soc., Dalton Trans.* **1987**, 1157–1161. (b) Hayami, S.; Matoba, T.; Nomiyama, S.; Kojima, T.; Osaki, S.; Maeda, Y. *Bull. Chem. Soc. Jpn.* **1997**, *70*, 3001–3009. (c) Pritchard, R.; Barret, S. A.; Kilner, C. A.; Halcrow, M. A. *J. Chem. Soc., Dalton Trans.* **2008**, 3159–3168.

SCO chemistry of iron complexes.[24] In manganese chemistry, the Schiff base ligand tends to stabilize the ion in its Mn^{III} oxidation state, which is known to be HS in a vast majority of cases ($S = 2$, ^5E_g in octahedral reference). In spite of the general scarcity of manganese(III) SCO reports along the time line, one notes two remarkable recent experimental studies.[25] Thus, Morgan et al.[25a] reported the crystal structure of a manganese(III) bifunctional Schiff base complex, which shows a gradual SCO phenomenon. Another very interesting case is that of a manganese(III) complex with a tridentate ligand having the N_2O donor set resulting from a Schiff function, a pyridine moiety, and one ionized alcohol oxygen donor.[25b] This ligand coordinates in a facial manner, yielding a *trans*-N_4O_2 total donor set, with the complex showing also gradual SCO.

All of the known manganese(III) SCO studies are basically only experimental, with many questions with regard to the factors of the spin-state interconversion in manganese(III) systems remaining to be answered by theoretical advances. In order to understand the manganese(III) SCO from a microscopic view, we use the opportunity of our recent synthetic findings to challenge the related advanced questions of this issue. We hereby report the structure, the temperature dependence of the magnetic susceptibility of a manganese(III) Schiff base complex with SCO behavior, and its detailed theoretical analysis. Spectral, electrochemical, and kinetic studies of this complex have been carried out previously.[26] However, the crystal structures and magnetic properties, i.e., the most important experimental evidence, have not been previously clarified. The presented complex has the interesting feature of a single hexadentate ligand wrapping the metal ion into a distorted octahedral pattern. The strain resulting from the "mechanical" limitation of the ligand in matching the ideal octahedron may play a role in triggering the dynamics related with the spin-conversion effects.

Most of the existing theoretical studies on spin transition[27] are dedicated to iron systems, in parallel with the prevalence of the iron(II) complexes among the reported SCO articles. To our best knowledge, this is the first manganese(III) SCO system analyzed with a combined account of experimental and computational data. Having rare occurrence, the manganese(III) spin transition does not benefit from the attention of theoretical analysis. The density functional theory (DFT) calculations, interpreted in terms of the ligand-field theory, were oriented to offer answers in the language of chemical intuition. The key parameters of the mechanisms were addressed with the help of properly settled computational experiments.

Experimental Section

Materials and Physical Measurements. *N*,*N*′-Bis(3-aminopropyl)ethylenediamine, 5-bromosalicylaldehyde, and manganese(III) perchlorate hexahydrate were purchased from Aldrich. All other reagents were purchased from standard sources and used as received. The IR spectra were recorded on a Nicolet-170SX FTIR spectrophotometer with KBr pellets in the range 4000−400 cm^{-1}. Elemental analyses for carbon, hydrogen, and nitrogen were performed on a Perkin-Elmer 240C analyzer. Variable-temperature magnetic susceptibility data were collected using a Quantum Design MPMS SQUID magnetometer. The experimental susceptibilities were corrected for the diamagnetism of the constituent atoms (Pascal's constants). ***Caution!*** *Although we have experienced no difficulties with the perchlorate salts, these should be regarded as potentially explosive and handled with care*.

Preparation of the [Mn(5-Br-sal-N-1,5,8,12)]ClO_4 Complex. *N*,*N*′-Bis(3-aminopropyl)ethylenediamine (0.54 g, 3.1 mmol) was added to a solution of 5-bromosalicylaldehyde (1.31 g, 6.5 mmol) in ethanol (25 mL), followed by solid $Mn(ClO_4)_2 \cdot 6H_2O$ (1.09 g, 3 mmol). The solution was heated to reflux for 20 min and filtered while hot. Dark-brown crystals formed on cooling. Yield: 850 mg (41%). Anal. Calcd for $C_{22}H_{26}Br_2ClMnN_4O_6$: C, 38.15; H, 3.78; N, 8.09%. Found: C, 38.18; H, 3.87; N, 8.07%.

Crystallographic Data Collection and Refinement of the Structure. Data for the compound were collected by a Bruker SMART APEX diffractometer employing graphite-monochromated Mo Kα radiation ($\lambda = 0.710\,73$ Å) at temperatures of 100 and 294 K. The data integration and reduction were undertaken with *SAINT* and *XPREP*.[28] The structure was solved by direct methods using *SHELXS-97*[29] and refined using least-squares methods on F^2 with *SHELXL-97*. Non-hydrogen atoms were modeled with anisotropic displacement parameters, and hydrogen atoms were placed by differential Fourier synthesis and refined isotropically. Crystal data of [Mn(5-Br-sal-N-1,5,8,12)]-ClO_4 at 100 K, HS and LS: $C_{22}H_{26}Br_2ClMnN_4O_6$, $M = 692.68$, monoclinic space group $P2/c$, $a = 17.6307(16)$ Å, $b = 8.0827(7)$ Å, $c = 18.1802(17)$ Å, $\beta = 94.918(2)°$, $V = 2581.2(4)$ Å^3, $Z = 4$. A total of 18 212 reflections were collected ($2.29° < \theta < 27.51°$), of which 5933 unique reflections ($R_{int} = 0.0658$) were measured. Residual R and wR were 0.0347 and 0.0922, respectively, from refinement on F^2 with $I > 2\sigma(I)$. At 294 K, HS and HS: $C_{22}H_{26}Br_2ClMnN_4O_6$, $M = 692.68$, monoclinic space group $P2/c$, $a = 17.8290(3)$ Å, $b = 8.2279(18)$ Å, $c = 18.1360(4)$ Å, $\beta = 94.073(12)°$, $V = 2653.7(10)$ Å^3, $Z = 4$. A total of 26 602 were collected ($2.29° < \theta < 27.51°$), of which 6086 unique reflections ($R_{int} = 0.0709$) were measured. Residual R and wR were 0.0560 and 0.1251, respectively, from refinement on F^2 with $I > 2\sigma(I)$.

Computational Methods. DFT calculations were carried out with the Amsterdam Density Functional (ADF) package,[30] using triple-ζ polarized basis sets (TZP) and Becke−Perdew functionals.[31] Technical facilities specific to the ADF code (fragment energy analysis and fractional and non-*aufbau* orbital populations)[32] afforded the outlined numerical experiments on the different configurations relevant for the spin-transition mechanism.

(24) (a) Weber, B.; Kaps, E.; Weigand, J.; Carbonera, C.; Letard, J. F.; Achterhold, K.; Parak, F. G. *Inorg. Chem.* **2008**, *47*, 487–496. (b) Weber, B. *Coord. Chem. Rev.* **2009**, *253*, 2432–2449.

(25) (a) Morgan, G. G.; Murnaghan, K. D.; MüllerBunz, H.; McKee, V.; Harding, C. J. *Angew. Chem., Int. Ed.* **2006**, *45*, 7192–7195. (b) Liu, Z.; Liang, S.; Di, X.; Zhang, J. *Inorg. Chem. Commun.* **2008**, *11*, 783–786.

(26) Panja, A.; Shaikh, N.; Gupta, S.; Butcher, R. J.; Banerjee, P. *Eur. J. Inorg. Chem.* **2003**, 1540–1547.

(27) Paulsen, H.; Trautwein, A. X. In Spin crossover in Transition Metal Compounds III. *Topics in Current Chemistry*; Gülich, P., Goodwin, H. A., Eds.; Springer-Verlag: Berlin, 2004; Vol. *235*, pp 197−219.

(28) *SMART, SAINT, and XPREP, area detector control and data integration and reduction software*; Bruker Analytical X-ray Instruments Inc.: Madison, WI, 1995.

(29) Sheldrick, G. M. *SHELX97, Programs for Crystal Structure Analysis*; University of Göttingen: Göttingen, Germany, 1998.

(30) (a) *ADF2006.01, SCM, Theoretical Chemistry*; Vrije Universiteit: Amsterdam, The Netherlands, http://www.scm.com. (b) te Velde, G.; Bickelhaupt, F. M.; van Gisbergen, S. J. A.; Fonseca Guerra, C.; Baerends, E. J.; Snijders, J. G.; Ziegler, T. *J. Comput. Chem.* **2001**, *22*, 931–967. (c) Fonseca Guerra, C.; Snijders, J. G.; te Velde, G.; Baerends, E. J. *Theor. Chem. Acc.* **1998**, *99*, 391–403.

(31) (a) Becke, A. D. *Phys. Rev. A* **1988**, *38*, 3098–3100. (b) Perdew, J. P. *Phys. Rev. B* **1986**, *33*, 8822–8824. (c) Perdew, J. P. *Phys. Rev. B* **1986**, *34*, 7406.

(32) te Velde, G.; Bickelhaupt, F. M.; Baerends, E. J.; Fonseca Guerra, C.; Van Gisbergen, S. J. A.; Snijders, J. G.; Ziegler, T. *J. Comput. Chem.* **2001**, *22*, 931–967.

Scheme 2

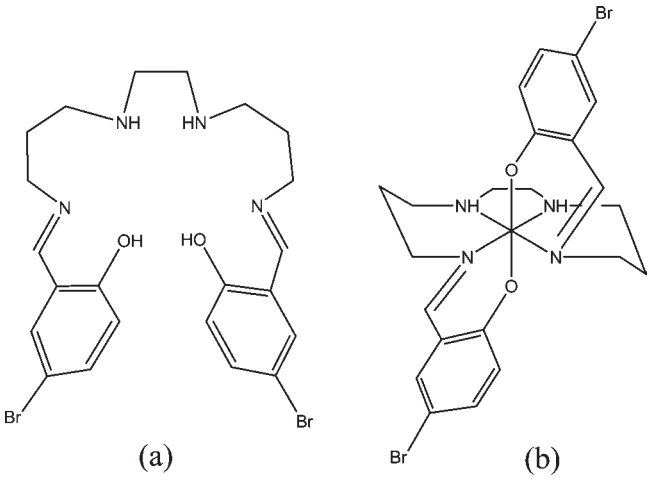

Results and Discussion

Description of the Structures. As was preliminarily pointed in the Introduction and is detailed in the forthcoming discussion, a key feature in the occurrence of a SCO manifestation for the presented manganese(III) complex is the nature of the ligand, which ensures a strong ligand field and assists, by its vibrational properties, the dynamics of the spin conversion. Scheme 2 represents the constitution of the hexadentate Schiff base ligand and the formal topology of the complex.

The crystals of the [Mn(5-Br-sal-N-1,5,8,12)]ClO_4 complex, deposited from a methanol/ethanol solution, are black rectangular-shaped blocks. The X-ray data collection was performed on the same crystal at room temperature and 100 K. A summary of the crystallographic details of the X-ray analyses of the manganese(III) compounds is given in the Experimental Section. Selected bond distances and angles are supplied in Table 1. The crystal structure of the [Mn(5-Br-sal-N-1,5,8,12)]-ClO_4 molecular unit is represented in Figure 1. At both temperatures (294 and 100 K), it contains two crystallographically independent mononuclear manganese(III) complex cations (Mn1 and Mn2) in the asymmetric unit. The complexes are roughly similar, differing incrementally in their geometry parameters. The complex units are pseudo-octahedral and quasi-tetragonal, with two oxygen donors oriented trans to each other and four nitrogen atoms in an approximate equatorial plane. A 2-fold rotation axis through the manganese center bisects the C−C linkage of the ethylenediamine moiety at the middle of the ligand. This generates geometrically equivalent pairs of *cis*-amine (N2 and N2A; N4 and N4A), *cis*-imine (N1 and N1A; N3 and N3A), and *trans*-phenolate (O1 and O1A; O2 and O2A) donors. The average Mn−L bond distances [for complex cation 1, Mn1−O1 = 1.865(3) Å, Mn1−N1 = 2.107(3) Å, and Mn1−N2 = 2.215(4) Å; for complex cation 2, Mn2−O2 = 1.869(3) Å, Mn2−N3 = 2.086(4) Å, and Mn2−N4 = 2.184(4) Å] show that both complex cations in the structure at 294 K are purely HS ($S = 2$).

Table 1. Selected Bond Distances (Å) and Angles (deg) for [Mn(5-Br-sal-N-1,5,8,12)]-ClO_4, Taken Comparatively at 294 K (Both Manganese Sites in the HS State) and 100 K (Mn1 in the HS State and Mn2 in the LS State)[a]

	294 K	100 K
	Bond Distances	
Mn1−O1	1.865(3)	1.867
Mn1−N1	2.107(3)	2.110
Mn1−N2	2.215(4)	2.220
Mn2−O2	1.869(3)	1.881
Mn2−N3	2.086(4)	1.999
Mn2−N4	2.184(4)	2.060
	Bond Angles	
O1−Mn1−O1A	178.92(18)	179.34(18)
O2−Mn2−O2A	179.6(2)	176.83(19)
N1−Mn1−N2	163.72(14)	163.26(14)
N3−Mn2−N4	165.65(16)	171.48(16)
O1−Mn1−N1	87.03(12)	87.21(13)
O1−Mn1−N1A	92.35(13)	92.41(13)
O1−Mn1−N2	94.00(14)	93.92(14)
O1−Mn1−N2A	86.82(14)	86.59(14)
N1−Mn1−N2	84.66(14)	84.83(14)
N1−Mn1−N1A	110.65(19)	110.96(19)
N2−Mn1−N2A	80.7(2)	80.1(2)
O2−Mn2−N3	86.17(13)	88.67(14)
O2−Mn2−N3A	93.54(14)	93.41(14)
O2−Mn2−N4	92.76(16)	91.79(15)
O2−Mn2−N4A	86.92(15)	85.87(15)
N3−Mn2−N4	86.17(16)	88.75(16)
N3−Mn2−N3A	107.1(2)	98.1(2)
N4A−Mn2−N4	81.3(2)	84.9(3)

[a] The temperature-dependent measurements were taken on the same single crystal.

Considering that a change in the ground state has sizable consequences in the molecular geometry, the SCO can be unequivocally detected by single-crystal X-ray crystallography.[33] The SCO phenomenon can even be roughly measured by the unit cell volume changes, which are sensibly larger[34] than the usual slight dependence of the volume with the temperature. In our case, the volume is 2653.7 $Å^3$ at room temperature and decreases to 2581.2 $Å^3$ at 100 K. This is in line with the molecular volume variation because HS complexes appearing at higher temperature are expected to display larger radii than their LS congeners. Aside from the overall change of the coordination bond lengths with the SCO event, one may expect subtle geometry changes in each state because of more specific effects. Namely, the HS manganese(III) complexes are known to be prone to Jahn−Teller distortions because of the ^5E degenerate state in the octahedral reference.[35] In quasi-octahedral systems, the distortion may still effectively take place because of pseudo Jahn−Teller forces that drive the system, usually to elongated octahedra. The presented complex unit is apparently a bit

(33) (a) Sunatsuki, Y.; Ikuta, Y.; Matsumoto, N.; Ohta, H.; Kojima, M.; Iijima, S.; Hayami, S.; Maeda, Y.; Kaizaki, S.; Dahan, F.; Tuchagues, J.-P. *Angew. Chem., Int. Ed.* **2003**, *42*, 1652–1656. (b) Tanimura, K.; Kitashima, R.; Bréfuel, N.; Nakamura, M.; Matsumoto, N.; Shova, S.; Tuchagues, J.-P. *Bull. Chem. Soc. Jpn.* **2005**, *78*, 1279–1282. (c) Breuning, E.; Ruben, M.; Lehn, J.-M.; Renz, F.; Garcia, Y.; Ksenofontov, V.; Gutlich, P.; Wegelius, E.; Rissanen, K. *Angew. Chem., Int. Ed.* **2000**, *39*, 2504–2507.

(34) (a) Thompson, A. L.; Goeta, A. E.; Real, J. A.; Galet, A.; Muñoz, M. C. *Chem. Commun.* **2004**, 1390–1391. (b) Matouzenko, G. S.; Bousseksou, A.; Borshch, S. A.; Perrin, M.; Zein, S.; Salmon, L.; Molnar, G.; Lecocq, S. *Inorg. Chem.* **2004**, *43*, 227–236. (c) Pillet, S.; Hubsch, J.; Lecomte, C. *Eur. Phys. J. B* **2004**, *38*, 541–552. (d) Yamada, M.; Ooidemizu, M.; Ikuta, Y.; Osa, S.; Matsumoto, N.; Iijima, S.; Kojima, M.; Dahan, F.; Tuchagues, J.-P. *Inorg. Chem.* **2003**, *42*, 8406–8416.

(35) Krivokapic, I.; Noble, C.; Klitgaard, S.; Tregenna-Piggott, P.; Weihe, H.; Barra, A.-L. *Angew. Chem., Int. Ed.* **2005**, *44*, 3613–3616.

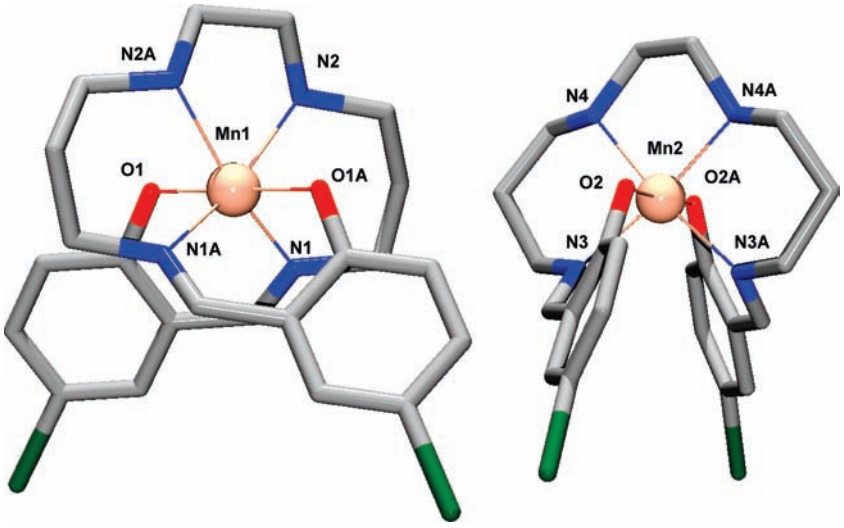

Figure 1. View of the complex cations in the X-ray crystal structure of [Mn(5-Br-sal-N-1,5,8,12)]ClO_4 at 100 K. The system at 294 K is visually and qualitatively similar, with the slight geometry differences being comparatively outlined in Table 1.

unusual from this point of view also, displaying compression along the O−Mn−O axial direction. The coordination sphere change under the SCO event is not isotropic. In the cooling mode, along with the significant shortening of all four Mn−N bond lengths, the axial Mn−O bond lengths remain almost unchanged.

Another interesting structural particularity is the fact that only one of the slightly different $[Mn(5\text{-Br-sal-N-}1,5,8,12)]^+$ units undergoes the spin transition. As a consequence, at 100 K, one of the two complex cations (Mn1 site) is in the HS state and the other (Mn2 site) is in the LS state. The bond distances of the HS complex cation (Mn1 site) are crystallographically indistinguishable from those of the two HS complex cations at 294 K (Table 1). The average Mn−L bond distances in the HS complex cation (Mn1) is 2.066 Å, whereas in the LS complex cation is 1.980 Å. This gives an average difference of 0.09 Å. Despite the growing interest in the use of variable-temperature X-ray analysis to monitor spin transitions in SCO systems, observation of crystallographically independent pure HS and LS metal centers for a given mononuclear manganese(III) complex at the same temperature remains an extremely rare occurrence. Commonly, in mononuclear iron(III) and iron(II) cases where two crystallographically distinct molecules coexist, two scenarios are possible: (i) both metal centers are HS[36] or LS;[37] (ii) the spin state at each center is impure.[38] Recently, Shongwe et al. reported an iron(III) complex that consists of two distinct HS and LS complex cations in the asymmetric unit.[39a] The cases of differentiated spin behavior as a function of the crystallographic particularities are rather frequent and diverse, with another particular case being those of iron(II) systems showing gradual conversion at one site and firm spin transition at others.[39b] However, manganese(III) systems with such particularities were not previously reported.

The analysis of the crystal packing suggests the reasons for the different spin behaviors of the Mn1 vs Mn2 sites. The packing diagrams for $[Mn(5\text{-Br-sal-N-}1,5,8,12)]ClO_4$ at 100 and 294 K are given in Figures 2 and 3, respectively. One observes that the manganese(III) complexes are organized in chains, one type for each crystallographic species. In each chain, the enantiomeric units of the same crystallographic species are alternating in a zigzag pattern. The perchlorate counterions establish many hydrogen bonds throughout the crystal, interlinking coordination cations of the same type or belonging to the two different sorts. As Figure 2 shows, the network of links mediated by perchlorate seems denser in the Mn1 chains, which do not undergo spin conversion. Besides, in this case, one may observe a stacking of phenyl groups from ligands of neighboring units (in an enantiomeric relationship). One may speculate then that this chain is more rigid because of tighter packing, and possibly this prevents the occurrence of spin transition along it. More precisely, the stacking hinders the flexibility of the whole ligand, precluding the spin transformation of the Mn1 site. On the other hand, the intermolecular interactions are essential for the cooperativity of the SCO effect, helping to transform it in a sudden phase transition. The perchlorate intermediate linking among the Mn2 sites is relatively weak (hydrogen bonds of C−H···O and N−H···O types), being not sufficient to establish a very good cooperativity, which would determine a steep process and the hysteresis. By a comparison of the above-described slightly different situations, one realizes the very subtle balance of the supramolecular effects that, over small thresholds, can either favor or prevent a molecular SCO process. Other graphic representations detailing the molecular and crystal structures are given in the Supporting Information.

Magnetic Properties. The SCO behavior is primarily analyzed by using variable-temperature magnetic susceptibility measurements. Figure 4 displays the effective magnetic moment related with two molecular units of the $[Mn(5\text{-Br-sal-N-}1,5,8,12)]ClO_4$ compound. At room

(36) Hayami, S.; Gu, Z.; Shiro, M.; Einaga, Y.; Fujishima, A.; Sato, O. *J. Am. Chem. Soc.* **2000**, *122*, 7126–7127.
(37) Juhász, G.; Hayami, S.; Sato, O.; Maeda, Y. *Chem. Phys. Lett.* **2002**, *364*, 164–170.
(38) Conti, A. J.; Chadha, R. K.; Sena, K. M.; Rheingold, A. L.; Hendrickson, D. N. *Inorg. Chem.* **1993**, *32*, 2670–2680.
(39) (a) Shongwe, M. S.; Al-Rashdi, B. A.; Adams, H.; Morris, M. J.; Mikuriya, M.; Hearne, G. R. *Inorg. Chem.* **2007**, *46*, 9558–9568. (b) Reger, D. L.; Gardinier, J. R.; Gemmill, W. R.; Smith, M. D.; Shahin, A. M.; Long, G. J.; Rebbouh, G.; Grandjean, F. *J. Am. Chem. Soc.* **2005**, *127*, 2303–2316.

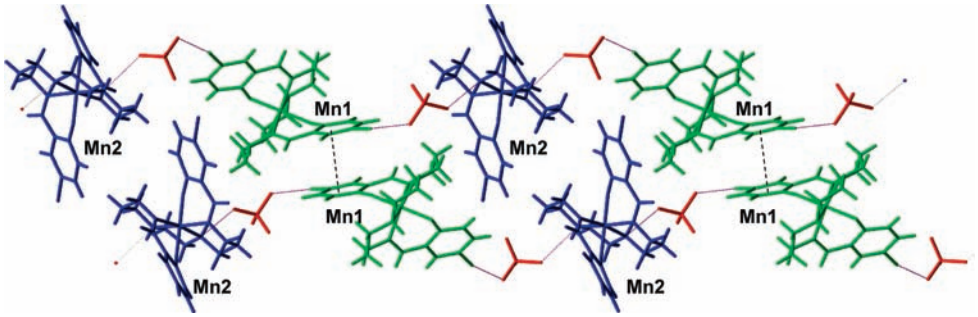

Figure 2. View of packing in the X-ray crystal structure of [Mn(5-Br-sal-N-1,5,8,12)]ClO_4 at 100 K. The Mn1 units (having no spin-conversion effect, here in HS state) are green (light), while the Mn2 units (with spin conversion, here in the LS form) are blue (dark). Only part of the intermediate linking by perchlorate−ligand hydrogen bonds is figured. One observes a stacking effect between ligands of the Mn1 units.

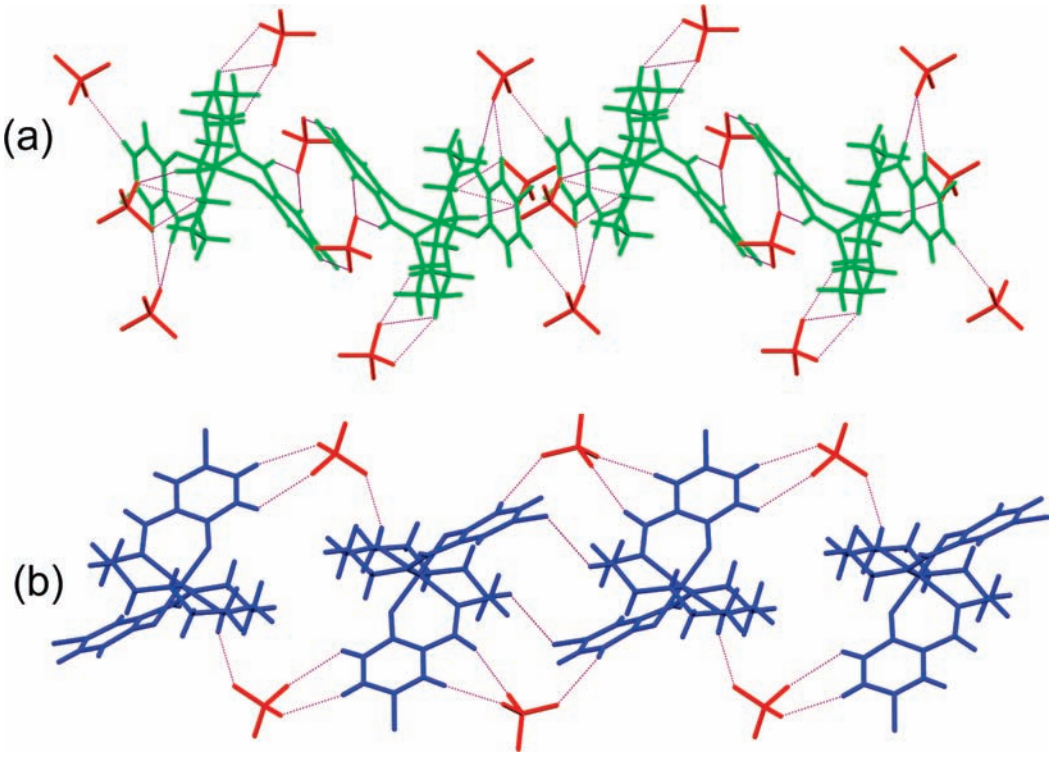

Figure 3. Details of packing in the crystal structure of [Mn(5-Br-sal-N-1,5,8,12)]ClO_4 at 294 K. The separated chains of the Mn1 (a) and Mn2 (b) units (not in a relative placement from the crystal) are shown. One notes that the chain of Mn1-type complexes has more perchlorate-mediated intermolecular links.

temperature, the maximum value is 6.6 μ_B, pointing to the existence of two HS sites. The value of μ_{eff} declines slowly upon cooling, tracing a quasi-constant plateau, down to about 258 K and then undergoes a rather steep, tough, gradual decrease, marking the spin-conversion event. The minimal μ_{eff} is 5.60 μ_B at 50 K, a low-temperature approximate plateau corresponding to the sum of one HS and one LS manganese(III) unit. The gradual transformation and the coincidence of the curves in heating versus cooling modes show the absence of thermal hysteresis. In the attempt to treat the μ_B vs T curve by numerical integration in the frame of nonisothermal kinetics, we found that the overall fit can be realized only with nonreasonable preexponential factors. This shows that the conversion has an intrinsic quantum nature and its dynamics cannot be treated in the simplified frame of formal kinetics.[40] However, for the sake of a rough estimation, we retrieved the activation energy by fitting the position of the maximum reaction speed (the inflection point of the μ_B vs T curves) under the imposed hypothesis of an ideally unimolecular process with Arrhenius factor $A = 10^{11}$ s^{-1}. This gave an activation energy of about $E_a = 2400\ cm^{-1}$ (6.7 kcal/mol), comparable with other SCO kinetic analyses.[40] It is interesting to observe also that this amount is in the range notoriously acknowledged for hydrogen bonding. Then, one may speculate that the hydrogen-bonding network noticed in the crystal structure can intervene in the process, assisting or triggering, at the supramolecular level, the molecular transformation.

Electron Structure Studies. The Ligand-Field Orbital Sequence. Complementary to experimental techniques and the phenomenological perspective, electronic structure calculations in the frame of DFT[41] were employed.

(40) Linert, W.; Grunert, M. C.; Koudriavtsev, A. B. *Top. Curr. Chem.* **2004**, *235*, 105–136.

(41) Koch, W.; Holthausen, M. C. *A Chemist's Guide to Density Functional Theory*; Wiley-VCH GmbH: Weinheim, Germany, 2001.

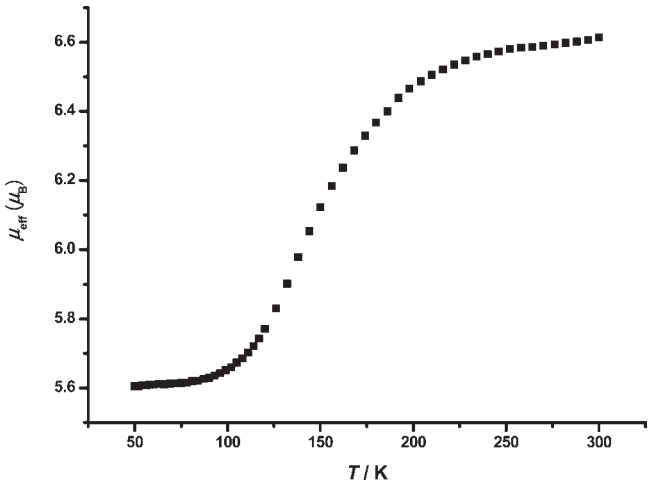

Figure 4. Variation of the magnetic moments of [Mn(5-Br-sal-N-1,5,8,12)]ClO_4 with temperature, related with respect to two molecular units (Mn1, HS in the entire temperature range; Mn2, undergoing a transition from LS at low T to HS at higher T).

The aim of the calculations is to obtain a heuristic insight into the mechanism and key parameters of the experimentally revealed case study. The electron structure methods have been used to study SCO systems in general,[27] most of them dealing with iron or cobalt complexes. To the best of our knowledge, no study devoted to the manganese(III) spin conversion is known. The general reliability of DFT for the account of spin-transition gaps was discussed in several studies devoted to iron complexes.[42] Thus, systematic assessments of the basis set or functional dependences, as well as comparisons of different codes, along with detailed introductory issues, gave a pedantic favorable report for most of the available DFT technical varieties.[42b] Our clue is rather different, conceiving the use of calculations in semiquantitative respects. A detailed analysis of the numeric effects of functional and basis set tuning in the particular case of manganese(III) complexes is not our actual focus. We conventionally confine to the setting mentioned in the paragraph on the previous methods. The subsequent conclusions proved in the end that this offered a reasonable description of the physical parameters.

The used ADF package[30] afforded the possibility to control, by input, the electron and spin population in selected orbitals, affording also fractional and non-*aufbau* configurations.[32] This is very useful in mimicking different situations that can be related with the mechanism of the investigated spin transition. For instance, the fractional occupation allows one to tackle degenerate or quasi-degenerate orbital sets, a result of a certain occupation scheme having, in terms of ligand-field translation, the meaning of the corresponding average over various spectral terms resulting from the given configuration.[43] Another useful feature of ADF is the possibility of working with predefined fragments such as the metal ions and ligands, affording output readable in the key of chemical intuition, offering information somewhat comparable with the virtues of postcalculation charge density analyses.[44]

Previous ADF studies devoted to spin transition in iron complexes, even employing in certain circumstances the fractional occupation numbers, do not use the full conceptual leverage of this technique.[42b] Interesting analyses based on controlled orbital populations treated the theoretical possibility of spin transition in $[M_2Cl_9]^{3-}$ (M = Fe, Ru, Os) face-shared bioctahedral complexes.[45] A series of $[M_2X_9]^{3-}$ and $[M_3X_{12}]^{3-}$ complexes were analyzed in various magnetostructural respects,[46] by similar techniques, implicitly using the specific advents of the ADF code. However, the theoretical schemes used in the abovecited works differ from our actual use of controlled orbital and spin populations. Our procedures, though simple, are the first attempts to use occupation-tuned DFT calculations to extract the parameters for the ligand-field splitting and spin-pairing energy magnitudes in SCO complexes. This sort of insight is richer than the simple DFT calculation of orbital diagrams or the estimation of the HS−LS total energy gaps.

Aiming a "blank" reference, which eliminates, by design, the differentiated role of spin effects, we carried out a restricted-type calculation of a system having enforced equal populations over the frontier molecular orbitals (MOs) associated with the ligand-field scheme. This helps us to keep a unified view of the interpretations based on orbital pictures because, otherwise, even conserving a certain qualitative pattern, the detailed shape of the orbitals may show a certain dependence on the geometry, occupation, and spin balance. The conventional unique reference is obtained by a calculation averaging four electrons originating from the valence shell of manganese(III) over the last five MOs with appropriate symmetry, i.e., having the $^4/_5 = 0.8$ electron population in each of them. The orbitals obtained in this way show the following energy ordering sequence 75a < 73b < 76a < 74b < 77a, with respect to the C_2 symmetry of the molecular unit. The first three orbitals correspond to the $t_{2g} \rightarrow$ 2a + b split, at the $O_h \rightarrow C_2$ symmetry lowering, with the last two belonging to the $e_g \rightarrow$ a + b reduction. The structure corresponded to the geometry optimized under the $(75a)^{0.8}(73b)^{0.8}(76a)^{0.8}(74b)^{0.8}(77a)^{0.8}$ average configuration. To avoid possible confusion, we must point out that, in the frame of DFT, the fractional charges and spin and orbital populations are conceptually allowed.[47]

Also, for facilitation of a qualitative interpretation, we define a convenient molecular orientation. According to the standard convention for the point groups, the z direction must be chosen along the main rotation axis, C_2 in our case. This is the line bisecting the N(imine)−Mn−N(imine) and N(amine)−Mn−N(amine) angles. However, this standard choice may be a bit confusing in the attempt to interpret the orbital composition of d-type functions in

(42) (a) Paulsen, H.; Trautwein, A. X. *J. Phys. Chem. Solids* **2004**, *65*, 793–798. (b) Daku, L. M. L.; Vargas, A.; Hauser, A.; Fouqueau, A.; Casida, M. E. *Chem. Phys. Chem.* **2005**, *6*, 1393–1410.

(43) (a) Daul, C. *Int. J. Quantum Chem.* **1994**, *52*, 867–877. (b) Baerends, E. J.; Branchadell, V.; Sodupe, M. *Chem. Phys. Lett.* **1997**, *265*, 481.

(44) (a) Dapprich, S.; Frenking, G. *J. Phys. Chem.* **1995**, *99*, 9352–9362. (b) Gorelsky, S. I.; Solomon, E. I. *Theor. Chem. Acc.* **2008**, *119*, 57–65.

(45) Lovell, T.; Stranger, R.; McGrady, J. E. *Inorg. Chem.* **2001**, *40*, 39–43.

(46) (a) Cavigliasso, G.; Stranger, R. *Inorg. Chem.* **2003**, *42*, 5252–5258. (b) Cavigliasso, G.; Stranger, R. *Inorg. Chem.* **2008**, *47*, 3072–3083.

(47) (a) Gross, E. K. U.; Oliveria, L. N.; Kohn, W. *Phys. Rev. A* **1988**, *37*, 2809–2820. (b) Gross, E. K. U.; Oliveria, L. N.; Kohn, W. *Phys. Rev. A* **1988**, *37*, 2809–2820. (c) Ullrich, C. A.; Kohn, W. *Phys. Rev. Lett.* **2001**, *87*, 093001–093004. (d) Cances, E. *J. Chem. Phys.* **2001**, *114*, 10616–10621.

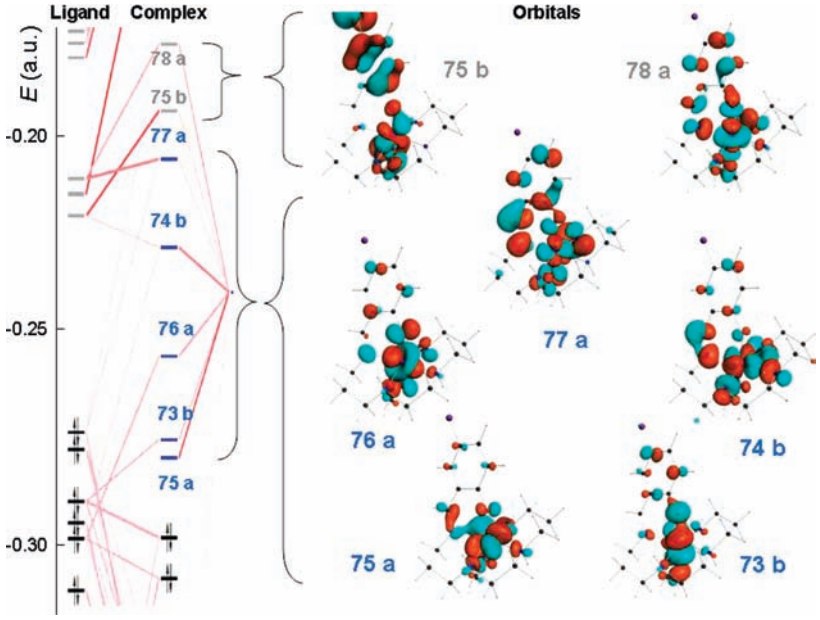

Figure 5. Frontier orbitals relevant for the ligand-field regime (having significant d-character content). The prediction resulted from restricted calculations with average orbital populations (four electrons over the last five MOs). Labels correspond to the C_2 symmetry. The composition of the orbitals with respect of a conventional octahedral reference is as follows: t_{2g}-type set, {75a ~ 65.10% xy + 6.85% yz, 73b ~ 29.58% yz + 26.68% xz, 76a ~ 34.02% xz + 15.39% yz}; e_g-type set, {74b ~ 43.23% $x^2 - y^2$, 77a ~ 14.59% z^2}. Significant d content is found also in the next virtual MOs: {75b ~ 17.40% $x^2 - y^2$, 78a ~ 36.99% z^2}. The outlined composition implied a conventional orientation of the reference frame, with the z axis oriented along the O−Mn−O moiety and the x and y axes close to the trans N−Mn−N directions.

relation to the customary labels of the octahedral frame. For a conventional compromise, one may then take an orthoaxial reference with the following orientation: the z axis parallel to the mean direction of the O−Mn−O quasi-linear fragment (the trans coordinating phenolates); the xy plane chosen in the mean {MnN_4} equatorial plane with x and y as close as possible to the N(imine)−Mn−N(amine) trans axes (recalling that the corresponding N−Mn−N angle deviates from the ideal 180° value). In this way, one may conveniently read the orbital composition given in the caption of Figure 5.

Figure 5 shows the corresponding sequence of MOs matching the ligand-field d-type components, as well as the two following virtual ones. The left side of Figure 5 shows the energies of the MOs from the ligand fragment, in relation to the MOs of the complex. The d character is smeared over several orbitals, beyond the five MOs of the nominal ligand-field sequence. Relatively important d traces are found also in the last few doubly occupied ligand-type MOs and in the first virtuals, suggesting the partly covalent nature of the coordination bonding. For instance, the second empty MO has a visible z^2 appearance. In turn, the last ligand-field-type MO, which may be qualitatively expected as z^2, has a mixed d-type content, showing one lobe along the z axis and another one between the x and y axes (with respect to the above-discussed conventional orientation). The mixed aspect comes from the actual distortion of the octahedral frame, causing a $\sigma-\pi$ combination, as a consequence of the low symmetry. The higher content of the ligand in the last occupied orbitals shows the role of charge transfer in the electron structure of the system.

The orbital groups traditionally ascribed to the t_{2g} and e_g octahedral parentages are not pure labels here. However, in qualitative respects, one may say that the actual ligand-field order reads here as follows: $xy < yz$, $xz < x^2 - y^2 < z^2$, in line with the compressed octahedral pattern. In fact, the last orbital is merely a ligand-based one, while the MO with the larger content in z^2 is a higher virtual orbital. Magnified MO pictures can be found in the Supporting Information.

Molecular Geometry Optimization. Structure as a Function of the Orbital and Spin Populations. The theoretical optimization of the molecular geometry as a function of the orbital and spin populations is illustrative numerical experiments. The computed geometries of the ground-state configurations are retrieving the experimental tendencies, testifying then the experimental assignment of the transition in terms of observed structure changes. The other considered occupation schemes can reveal, by corresponding handling, the electronic parameters of LFSE and spin pairing.

The differences in the bond lengths between the ^{5}A and ^{3}B ground states have the same magnitudes and patterns as those in the experimentally assigned HS and LS systems. Thus, the {ΔR_1, ΔR_2, ΔR_3} differences corresponding to the HS minus LS amounts for Mn−N(amine), Mn−N(imine), and Mn−O(phenolate) bond lengths, respectively, are {0.21, 0.12, −0.02} Å for the computed ^{5}A vs ^{3}B couple and {0.12, 0.09, −0.01} Å from the experiment. Except for a certain computational overestimation of the ΔR_1 element, the magnitudes and signs correspond to the experimental findings, offering also a theoretical confirmation for the interpretation attributed to the experimental facts. The structural changes in the equatorial plane are in good agreement with depopulation of the antibonding $x^2 - y^2$ orbital upon switching to the LS state, which results in a shorter equatorial distance. It is interesting to note the geometry variation obtained with the rather artificial experiment of the average spin

Table 2. Relative Energies and Corresponding Optimized Geometries Obtained from Various Computation Experiments on the Spin and Orbital Populations in the Sequence Determined by Ligand-Field and C_2 Actual Symmetry[a]

			coordination bond lengths (Å)			C_2 occupations of t_{2g}-like MOs			C_2 occupations of e_g-like MOs	
		relative energy (cm^{-1})	R_1	R_2	R_3	a	b	a	b	a
1	$(d_{av})^{AS}$	34410	2.26	2.03	1.88	0.4α, 0.4β	0.4α, 0.4β	0.4α, 0.4β	0.4α, 0.4β	0.4α, 0.4β
2	$R-(d_{av})^{HS}$	26638	2.17	2.00	1.89	0.5α, 0.5β	0.5α, 0.5β	0.5α, 0.5β	0.25α, 0.25β	0.25α, 0.25β
3	$R-(d_{av})^{LS}$	11255	2.10	1.97	1.93	$^2/_3\alpha$, $^2/_3\beta$	$^2/_3\alpha$, $^2/_3\beta$	$^2/_3\alpha$, $^2/_3\beta$	0	0
4	$U-(d_{av})^{HS}$	5593	2.20	2.08	1.98	1α	1α	1α	0.5α	0.5α
5	^5A	2653	2.31	2.10	1.89	1α	1α	1α	1α	0
6	^5B	6292	2.12	2.03	2.10	1α	1α	1α	0	1α
7	exp.		2.18	2.09	1.87					
8	$U-(d_{av})^{LS}$	4170	2.10	1.97	1.93	1α, $^1/_3\beta$	1α, $^1/_3\beta$	1α, $^1/_3\beta$	0	0
9	^3A	2645	2.11	1.98	1.94	1α	1α, 1β	1α	0	0
10	^3B	0	2.10	1.98	1.91	1α, 1β	1α	1α	0	0
11	exp.		2.06	2.00	1.88					

[a] The lowest energy, taken as zero of the scale, corresponds to the LS ^3B state. The bond length notations are as follows: R_1 = Mn−N(amine), R_2 = Mn−N(imine), R_3 = Mn−O(phenolate). The lines 1−3 correspond to restricted (spinless) calculations, while the other correspond to unrestricted treatments with corresponding HS or LS spin multiplicity. The ones labeled by (d_{av}) correspond to population smeared over all *d* orbitals, with the superscript AS in the first line marking the imposed spin average of α- and β-orbital populations.

populations, with the corresponding length differences taken from line 2 minus line 3 being {0.07, 0.03, −0.04} Å. Underestimating the equatorial displacements because of the imposed orbital average, this test shows the same pattern of variation, namely, that enlargement of the equatorial frame attracts, as a consequence, a slight compression of the axial coordination. This suggests that the pattern of geometry changes may be rather independent from particular orbital factors, being possibly because of other specifics such as the "elastic" response of the ligand as a whole, as described previously.

The series of restricted calculations (lines 1−3 in Table 2) correspond to an enforced elimination of spin polarization effects, taking equal α versus β occupancies ($S_z = 0$). Besides, line 1 also has an average imposed over all d orbitals. With these population schemes, one can infer various interesting quantities. Thus, the energy in line 1 minus the energy in line 2 or 3 yields the effective LFSE in HS versus LS, i.e., ∼7800 and ∼23 000 cm^{-1}, respectively. These quantities include the role of the geometry change, while they exclude, by a conventional average, the role of the spin.

We investigated the configurations leading to different symmetries, taking one A and one B orbital representation for each spin case (i.e., the ^5A, ^5B, ^3A, and ^3B series). These can be obtained by the corresponding occupation of the orbitals originating from the formal t_{2g} and e_g octahedral references. We also took, as a test, the average unrestricted calculation, which in the case of the HS system smears one α electron over the two orbitals with e_g parentage and in the case of the LS system spreads the β electron over the three components of the t_{2g} formal set (lines 4 and 8 in Table 2). The orbital ordering that determines the nature of the ground state can be a subject of subtle balance, while this kind of averaging discards, by design, such smaller details. The lowest energy in the presented series is obtained for the optimized ^3B ground state, which corresponds to the $(75a)^2(73b)^1(76a)^1$ configuration or, in rough sense (see the above considerations about "mixed" symmetry labels), to the $(xy)^2(yz)^1(xz)^1$ atomic orbital (AO) occupancy. The lowest HS term is ^5A, corresponding to the $(75a)^1(73b)^1$ $(76a)^1(74b)^1$ configuration, i.e., approximately to the $(xy)^1(yz)^1(xz)^1$-$(x^2-y^2)^1$ AO main part.

More data that help in suggesting a mechanism of the spin transition are presented in Figure 6. The energies of several configurations are drawn as a function of the SCO coordinate $\Delta R = R_{HS} - R_{LS}$, obtained by applying this generic difference to each Cartesian component of every atom. Besides, the states are computed at further deformed geometries, $R_{LS} - \Delta R$, situated on the left side of the figure, and $R_{HS} + \Delta R$, on the right side. The figured parabola are quantitative curves, passing through the described points of the defined reaction coordinate: $R_{LS} - \Delta R$, R_{LS}, R_{HS}, and $R_{HS} + \Delta R$. The activation energy can be roughly considered at the crossing point of the ^3B and ^5A curves, at about 3000 cm^{-1}, which is qualitatively consistent with the above kinetic estimation (2400 cm^{-1}). This crossing point is accidentally close to the energy of the ^3A excited state in the LS geometry, a fact that suggests the possible role of this level. The coupling between ^3B and the close ^3A electronic states of the LS molecule can occur via a deformation with *B* symmetry, promoted by thermal movements and perturbations from neighboring units in the crystal lattice. This vibrational−electron (vibronic or pseudo Jahn−Teller)[48] mechanism would be the low-symmetry correspondent of a formal Jahn−Teller effect that must occur in a $^3T_{1g}$ degenerate ground state of an octahedral LS manganese(III) unit.[49] The compressed octahedral pattern of our system is also a slightly nonusual situation because normally the Jahn−Teller effect leads to the axial elongation of manganese(III) complexes, with the opposite distortions being rare encounters.[50]

The symmetry of the electron−vibrational interaction, $(B\otimes A)_{electronic}\otimes B_{vibrational} = A$, provides a mechanism for encompassing the orbitally forbidden transition, with respect to the symmetry of the ground state (B in the LS

(48) Bersuker, I. B. *Chem. Rev.* **2001**, *101*, 1067–1114.
(49) (a) Atanasov, M.; Comba, P.; Daul, C. A.; Hauser, A. *J. Phys. Chem. A* **2007**, *111*, 9145–9163. (b) Atanasov, M.; Comba, P. *J. Mol. Struct.* **2007**, *838*, 157–163.
(50) Scheifele, Q.; Riplinger, C.; Neese, F.; Weihe, H.; Barra, A.-L.; Juranyi, F.; Podlesnyak, A.; Tregenna-Piggott, P. L. W. *Inorg. Chem.* **2008**, *47*, 439–447.

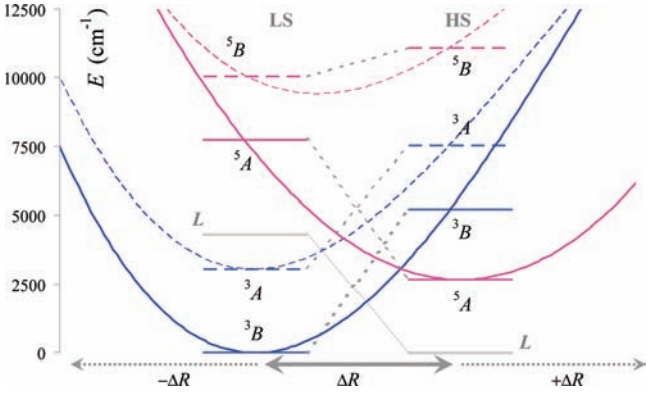

Figure 6. Scheme of the suggested mechanism of spin conversion based on the relative energies of various configurations computed for HS and LS molecular geometries. The relative energy of the ligand fragment, *L*, is represented with respect to its lowest value in the HS fragment. Therefore, the *L* labeled quantities have a different meaning (fragment energy, not a spectral term) and origin compared to all of the other represented levels, which have the meaning of ground and excited states measured with the relative zero at the ^{3}B (LS) level. The formal reaction coordinate ΔR is taken as the difference between the HS and LS geometries.

state and A in the HS one). The HS−LS process is spin-forbidden, with the driving force for this barrier being spin−orbit coupling. It is well-known from the attention devoted to the manganese(III) systems with single molecule magnet behavior[51] that this ion has strong magnetic anisotropy,[52] a characteristic that comes from spin−orbit determinations. Therefore, the acknowledged strong anisotropy of a Mn^{III} coordinated ion is a factor that assists the conversion process, providing mechanisms for lifting the spin barrier.

A detail helping us to understand other hidden forces of this process is the energy decomposition available in the ADF code, taking into account here the energy assignable to the ligand fragment. The ligand itself is about 4300 cm^{-1} richer in energy in the LS geometry than in the HS optimized geometry. A picturesque image on the ligand role (see the levels marked by *L* in Figure 6) is that its tension in the HS form stores enough energy to formally compensate for the gaps between the ^{3}B (LS) ground state and the ^{5}A (HS) one. The second derivative of energy with respect of the defined ΔR coordinate is higher for the ^{3}B ground state than for the ^{5}A one, at their respective minima. This quantity is parallel to the vibrational energy, being correlated with the fact that the molecular frame is more relaxed in the HS case. One may consequently say that, along the given reaction coordinate, the system "trades" electronic energy costs with gains in the vibrational freedom degrees. This perspective is paralleling, in microscopic terms, the thermodynamics language of enthalpy versus entropy factors. It is interesting also to note that the ^{3}A and ^{3}B curves (Figure 6) have almost coincident minima at the LS equilibrium geometry, while the ^{5}A and ^{5}B curves are quite different, the first corresponding to the HS point and the other being in between the HS and LS

(51) (a) Bagai, R.; Christou, G. *Chem. Soc. Rev.* **2009**, *38*, 1011–1026. (b) Gatteschi, D.; Sessoli, R. *Angew. Chem., Int. Ed.* **2003**, *42*, 268–297.

(52) (a) Ferbinteanu, M.; Miyasaka, H.; Wernsdorfer, W.; Nakata, K.; Sugiura, K.; Yamashita, M.; Coulon, C.; Clérac, R. *J. Am. Chem. Soc.* **2005**, *127*, 3090–3099. (b) Milios, C. J.; Vinslava, A.; Wernsdorfer, W.; Moggach, S.; Parsons, S.; Perlepes, S. P.; Christou, G.; Brechin, E. K. *J. Am. Chem. Soc.* **2007**, *129*, 2754–2755.

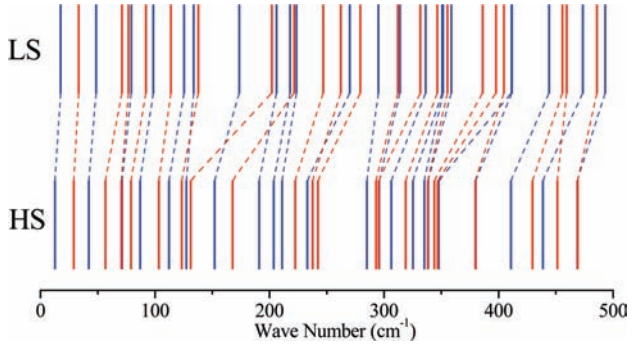

Figure 7. Computed vibration frequencies (sequence up to 500 cm^{-1}) for the HS (^{5}A) and LS (^{3}B) systems. The vibrations with *A* and *B* symmetries are in blue and red, respectively. Notice the shift of the LS spectrum at higher frequencies as compared to the HS one.

geometries, closer to the last one. Then, one may speculate that, if the system has been an elongated octahedron, with a ^{5}B groud state, the geometry changes upon spin transition were much smaller than the actual one. The geometry of a compressed octahedron seems then to be a key factor of the actual spin transition, besides the assistance offered by the elastic energy of the coordinated ligand.

Vibration Chemistry of the Spin-Transition Process. Another illustration of the above statements is realized by comparison of the computed vibration spectra (at the corresponding HS and LS optimized geometries, namely, those of the ^{5}A and ^{3}B states). In Figure 7, one may see the overall "blue" shift of the LS frequencies, as compared to the HS ones, as an illustration of the fact that the HS geometry has a lesser content of vibrational energy.

The analytical calculation of the vibration spectra afforded the zero-point energy (ZPE) correction of the total formation energies: $E = E_0 + E_{ZPE}$. The ZPE is simply the half-sum of all of the computed vibration energies.[53] With respect of the ZPE, the HS is lower in vibrational energy by $\Delta E_{ZPE} = -650$ cm^{-1}. As can be seen from Table 2 and Figure 6, with respect to the pure electronic part, the HS ground state is higher with $\Delta E_0 =$ 2653 cm^{-1} than the LS one. When the ZPE correction applied, the total HS−LS gap is lowered to $\Delta E = \Delta E_0 + \Delta E_{ZPE} \sim 2000$ cm^{-1}. Probably, the intermolecular effects (not accounted for in the actual modeling) are lowering more the effective gap, assisting the ligand in its noted trend to mechanical relaxation.

The vibration calculation afforded also an estimation of this part of the Hamiltonian into the thermodynamic quantities of the system. We excluded the contributions of the rotations and translation because the system is supposedly embedded in the solid network and these motions are hindered. However, the network is not inert and contributes in many subtle manners, via supramolecular interactions that cannot be accounted for here. In spite of the intrinsic incompleteness, it is important to note that the estimated $-T\Delta S_{vibr}$ part prevails, with its trend toward lower energies at growing *T*, against the ΔU_{vibr} one, which has the opposite variation (Figure 8). The simplistic account of the electronic part is the addition of the ΔE_0 gap to the internal energy and the $k_B \ln(5/3)$ to the

(53) Wilson, B. E., Jr.; Decius, J. C.; Cross, P. C. *Molecular vibrations*; Dover Publications: New York, 1980.

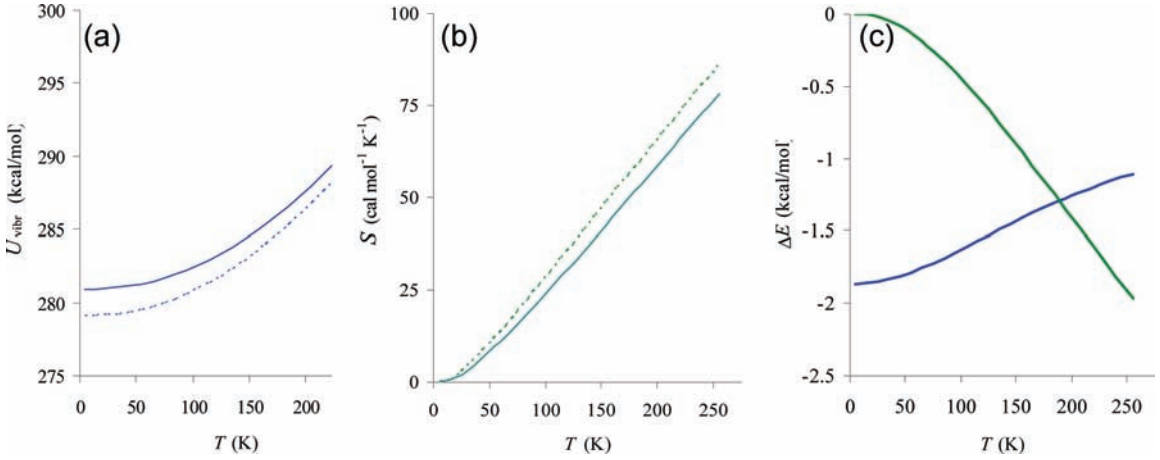

Figure 8. DFT estimation of the vibrational contribution to the thermodinamic quantities: (a) the vibrational internal energy U_{vibr}; (b) the entropy S; (c) the corresponding ΔU_{vibr} and the $-T\Delta S_{vibr}$ differences for the LS to HS process. In parts a and b, the LS system (^{3}B) is represented in a continuous line and the HS one (^{5}A) by a dashed curve. In part c, the difference is taken in the sense of HS minus LS. Note that these estimations do not retrieve the complete thermodynamics of the SCO process because the electronic part is not included.

entropy variation (with a number of microstates represented by multiplicities of quintet and triplet, respectively). The above estimation, $\Delta E_0 = 2653$ cm^{-1}, corresponds to about 7.6 kcal/mol, and the amended free energy $\Delta U - T\Delta S$ becomes positive, apparently not a satisfactory result. In fact, this suggests that one molecular unit is not sufficient to provoke a spin transition, with support of the complicated supramolecular effects being mandatory. We refrain from attempts of the computational estimation of intermolecular interactions, being aware that DFT has intrinsic limitations because of the improper design of usual functionals in the long-range limit, with the proper approach demanding the use of specialized techniques.[54]

Even though we cannot in this stage testify to such processes explicitly, one may speculate that the lattice effects can provide a further lowering by about 5 kcal/mol (i.e., an amount in the generic range of hydrogen bonding). Such a shift will amend the $\Delta U - T\Delta S$ curve (which already has a monotonous descending profile) in a way that provokes a sign switch from positive to negative (i.e., from thermodynamically forbidden to the allowed status) in the interval 50−200 K.

Searching for the Static Parameters of the Spin-Transition Effect. In this part, we will aim to retrieve from DFT calculations parameters relevant for the interpretation of our system in the frame of the ligand-field paradigm. The retrieval of simple concepts and parameters from the complexity of modern calculation is not simple, requiring particularly designed procedures, oriented to extract the ligand-field or magnetic Hamiltonian parameters.[55]

For the aimed purpose, we outlined the computational experiments presented in Table 3. Here the artificial geometry corresponding to the spin and orbital average calculations (i.e., the R_1-R_3 parameters of line 1 from Table 2) is kept frozen throughout a series of calculations. One may see that in this case the HS ^{5}A results as an absolute ground state. Compared to the ^{3}B geometry, the system shows a $\{\Delta R_1, \Delta R_2, \Delta R_3\}$ set with the $\{0.16, 0.05, -0.03\}$ values, which are intermediate to the variation at full transition between the ^{5}A and ^{3}B optimized systems. This can be taken conventionally as a sort of transition state, being placed at an intermediate position along the geometry deformation pattern and being optimized in conditions that are not specifically spin- and orbital-dependent. Keeping the given conventional geometry frozen, we can measure in qualitative conditions the LFSE and electron repulsion as parameters of the spin transition.

The fully averaged system has the highest energy for two reasons: it lacks the LFSE because of equal population over the five orbitals, and it experiences the highest electron repulsion because of the enforced pairing of the α and β fractional populations (0.4α and 0.4β in the same orbital). In qualitative terms, without detailing formulas and specific definitions, one may say that we have two kinds of electron repulsion: intraorbital, for the paired electrons accommodated in the same function, and interorbital, between electrons in different d-like functions, irrespective to their spin. The intra-orbital one is conceivably the highest because the electrons are enforced to closer encounters in the same region of the space. For the electrons (or a fraction of electron populations) placed in different orbitals and having the same spin, there is also a stabilization resulting from quantum exchange. Exchange and further effects from configuration interaction, called electron correlation, are generically accounted for, in certain limits, by the functionals used in the DFT calculations (in our case, the Becke−Perdew[31] approximation).

The lines 2 and 3 are measuring, in their absolute difference, ~13 000 cm^{-1}, the average energy cost of the spin pairing because part of LFSE is removed by averaging. The LFSE for HS ^{5}A is line 2 minus line 5, ~10 000 cm^{-1}, while for the LS ^{3}B, it comes from line 8 minus line 3, ~19 000 cm^{-1}. Comparing these two quantities, one may

(54) (a) Leininger, T.; Stoll, H.; Werner, H.-J.; Savin, A. *Chem. Phys. Lett*. **1997**, *275*, 151–160. (b) Sato, T.; Tsuneda, T. H. (c) Leininger, T.; Stoll, H.; Werner, H.-J.; Savin, A. *Chem. Phys. Lett*. **1997**, *275*, 151–160. (d) Sato, T.; Tsuneda irao, K. *Mol. Phys*. **2005**, *103*, 1151–1164. (e) Sato, T.; Tsuneda, T.; Hirao, K. *J. Chem. Phys*. **2007**, *126*, 234114.

(55) (a) Atanasov, M.; Daul, C. A.; Rauzy, C. *Chem. Phys. Lett*. **2003**, *367*, 737–746. (b) Atanasov, M.; Daul, C. A.; Rauzy, C. *Struct. Bonding* (*Berlin*) **2004**, *106*, 97–125. (c) Atanasov, M.; Comba, P.; Daul, C. A. *Inorg. Chem*. **2008**, *47*, 2449–2463.

Table 3. Relative Energies of Various Spin and Orbital Configurations Taken at the Conventional Optimized Geometry of the System with Average Orbital and Spin (Line 1 in Table 2 and the Present One)

				C_2 occupations of t_{2g}-like MOs			C_2 occupations of e_g-like MOs	
		spin S_z	relative energy (cm^{-1})	a	b	a	b	a
1	$(d_{av})^{AS}$	0	29339.5	0.4α, 0.4β	0.4α, 0.4β	0.4α, 0.4β	0.4α, 0.4β	0.4α, 0.4β
2	$U-(d_{av})^{HS}$	2	9962.0	0.8α	0.8α	0.8α	0.8α	0.8α
3	$U-(d_{av})^{LS}$	1	22818.4	0.6α, 0.2β	0.6α, 0.2β	0.6α, 0.2β	0.6α, 0.2β	0.6α, 0.2β
4	$U-(e_g)_{av}^{HS}$	2	3208.6	1α	1α	1α	0.5α	0.5α
5	^5A	2	0.0	1α	1α	1α	1α	0
6	^5B	2	6824.1	1α	1α	1α	0	1α
7	$U-(t_{2g})_{av}^{LS}$		5847.1	1α, $^1/_3\beta$	1α, $^1/_3\beta$	1α, $^1/_3\beta$	0	0
8	^3B	1	3008.9	1α, 1β	1α	1α	0	0
9	^3A	1	3854.1	1α	1α, 1β	1α	0	0

The meaning of the $U-(d_{av})$ labels is the same as that in Table 2; the $(e_g)_{av}$ and $(t_{2g})_{av}$ labels refer to the average of the switchable electrons (one α for HS or one β for LS) over the formal e_g or t_{2g} orbitals, respectively.

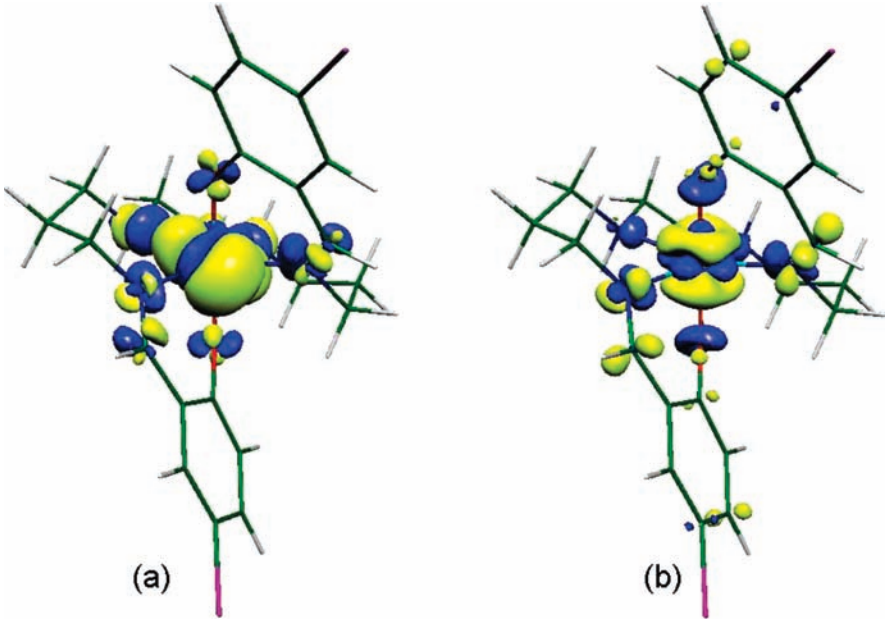

Figure 9. Total density difference maps taken for the (a) HS ^5A minus the LS ^3B densities and (b) for the average HS (one electron α delocalized on both e_g-like functions) against the average LS (one electron β delocalized over the three t_{2g}-like functions). The blue areas mark the accumulation of the electron density and the yellow ones the depletion in the areas from where the electron density was displaced.

see that the LS system benefits from a supplement of 9000 cm^{-1} in the LFSE. In the actual geometry, this cannot encompass the cost of the above-estimated spin pairing, ~13 000 cm^{-1}. Therefore, the system remains trapped in the HS state. One may see that the competing energies (LFSE vs pairing energy) are comparable, in the range of 10 000 cm^{-1}. A similar conclusion is reached, taking, as matter of convention, the average HS and LS states from lines 4 and 7. The average in this case is partial, over the e_g-type orbitals for the HS state and the t_{2g} ones for the LS state. For the specific couple of states, e.g., ^5A vs ^3B as above, the measured LFSE included the effects of the splitting inside the t_{2g} and e_g formal sets. The smearing over these two orbital sets of the electron switched in the transition process would give an average 10 *Dq*, which is about 10 000 cm^{-1}. The smearing brings the thought experiment closer to the octahedral reference. One obtains in this way the same qualitative understanding as that applied to the actual C_2 lower symmetry. Considering the other pair of states (^5B vs ^3A), one may verify the reverse situation, in which the LFSE difference (LS minus HS, ~15 800 cm^{-1}) compensates for the cost of electron pairing. However, this couple cannot be involved in spin transition because both states are excited ones.

Density Displacements. An interesting view of the spin transition is obtained with the help of total density maps and their difference (HS minus LS). The systems in Figure 9 are taken in the conditions of the calculations described in Table 3. Note that keeping the same conventional geometry in both HS and LS cases is important for catching the orbital effects only, without the implication of complexities related with the change of the molecular skeleton. Note also that we work now with the total density, not with the spin one.

Figure 9a shows the density difference taken for the "realistic" spin transition, ^5A vs ^3B. The density variation takes place approximately in the equatorial plane, explaining then why the most visible geometry change is recorded within this fragment, having smaller bond length displacements of the axial coordination. One may also see

that the density is removed from areas in between the ligands (yellow lobes) and concentrated along the coordination axes (blue lobes). In fact, this is similar to a $xy \rightarrow x^2 - y^2$ displacement that perfectly corresponds to the whole description of the coordination regime in the given complexes. In Figure 9b is illustrated a merely hypothetical spin transition effect, taken in the condition of the density-averaged electron (over t_{2g} like orbitals in the LS case and over the e_g ones in the HS case). In this case, we have a 3D image of a similar effect. The density is also removed from areas between ligands, which would correspond to the orientation of the lobes in the t_{2g} set, and brought near the metal−ligand axes, as expected for placement in the e_g set.

The spin density maps (shown in the Supporting Information) are qualitatively consistent with the above-discussed configurations approximated in terms of the main d AO weights: $(xy)^2(yz)^1(xz)^1$ for the LS case and $(xy)^1(yz)^1(xz)^1(x^2 - y^2)^1$ for the HS case. The LS map shows a visible spin-polarized pattern, having the bulk α spin density located on the metal ion, while the surrounding ligand lobes carry a residual β density.

Conclusion

Spin transitions in d^4 ions are rare events, with our results being an unedited contribution to the study of these sorts of systems. The particularities of the coordination sphere made with the actual ligand and the crystal-packing effects afforded the fulfillment of the subtle balance that forms the prerequisite of spin-conversion effects. An interesting effect demonstrating the narrow structural thresholds that favor the effect of spin conversion is the fact that only half of the Mn^{III} ions present in the lattice undergo the effect, as a consequence of slightly different packing conditions of the two crystallographic species. The computational experiments offered insight into the mechanisms of spin conversion, revealing different factors with the help of energy analyses in terms of ligand-field concepts. The geometry optimization, vibration analysis, and display of spin and density difference maps completed the tableau with an intuitive comprehension of the electronic structure factors. A key factor of the process is the strain contained in the coordinated ligand, higher in the LS form. Supposedly, its mechanical relaxation triggers the LS → HS process, with the onset of enhanced thermal movements. The compressed octahedral topology ensured by the hexadentate encapsulating ligand is favorable for the occurrence of spin-conversion effects. Further investigation into the new class of manganese(III) SCO systems with different counteranions and ligands is currently underway in our joint investigations.

Acknowledgment. S.W. gratefully acknowledges financial support from the Natural Science Foundations of China (Grant 20901042) and Jiangsu Province (Grant 09KJB150008). M.F. is indebted to the Romanian Ministry of Education and Research through CNCSIS Research Grant PCCE-239/2009. A.D. is partly supported by Grant PCE-174/2007. This work was also supported, in part, by the "National Basic Research Program of China" (2009CB930601).

Supporting Information Available: X-ray crystallographic file (CIF), additional structural, computational, and modeling details. This material is available free of charge via the Internet at http://pubs.acs.org.